Forest inventory stand height estimates from very high spatial resolution satellite imagery calibrated with LIDAR-plots

BRICE MORA[*1], MICHAEL A. WULDER[1], GEORDIE HOBART[1], JOANNE C. WHITE[1], CHRISTOPHER W. BATER[2], FRANCOIS A. GOUGEON[1], ANDRÉS VARHOLA[2], NICHOLAS C. COOPS[2]

[1] Canadian Forest Service (Pacific Forestry Centre), Natural Resources Canada, Victoria, British Columbia, Canada
[2] Department of Forest Resource Management, University of British Columbia, Vancouver, Canada

Key words: forest stand height, forest inventory, remote sensing, LIDAR, WorldView, panchromatic, object-based, monitoring

Running head: Stand height modelling using LIDAR data and VHSR imagery

Pre-print of published version.
Reference:
Mora, B., M.A. Wulder, G. Hobart, J.C. White, C.W. Bater, F.A. Gougeon, A. Varhola, N.C. Coops. (2013). Forest inventory stand height estimates from very high spatial resolution satellite imagery calibrated with LIDAR-plots. International Journal of Remote Sensing. Vol. 34, No. 12, pp. 4406–4424.
DOI.

http://dx.doi.org/10.1080/01431161.2013.779041

Journal link:
http://www.tandfonline.com/doi/abs/10.1080/01431161.2013.779041

ABSTRACT

Many areas of forest across northern Canada are challenging to monitor on a regular basis as a result of their large extent and remoteness. Although no forest inventory data typically exists for these northern areas, detailed and timely forest information for these areas is required to support national and international reporting obligations. We developed and tested a sample-based approach that could be used to estimate forest stand height in these remote forests using panchromatic Very High Spatial Resolution (VHSR, < 1 m) optical imagery and light detection and ranging (LIDAR) data. Using a study area in central British Columbia to test our approach, we compared four different methods for estimating stand height using stand-level and crown-level metrics generated from the VHSR imagery. "LIDAR-plots" (voxel-based samples of LIDAR data) are used for calibration and validation of the VHSR-based stand height estimates, similar to the way that field plots are used to calibrate photogrammetric estimates of stand height in a conventional forest inventory or to make empirical attribute estimates from multispectral digital remotely sensed data. A *k*-NN method provided the best estimate of mean stand height (R^2 = 0.69; RMSE = 2.3 m, RMSE-%=21) compared to linear regression, random forests, and regression tree methods. The approach presented herein demonstrates the potential of VHSR panchromatic imagery and LIDAR to provide robust and representative estimates of stand height in remote forest areas where conventional forest inventory approaches are either too costly or are not logistically feasible. Whilst further evaluation of the methods is required to generalize these results over Canada's northern forests, the synergistic use of VHSR and LIDAR data provides an opportunity for monitoring in areas that heretofore have had no detailed forest inventory information.

1. Introduction

Efficient forest management policies require robust estimates of stand height, as this parameter can be of importance for accurate stand volume and biomass derivation (Boudewyn *et al*. 2007), and site productivity estimation. The Canadian Forest Service (CFS) has the mandate to maintain a National Forest Inventory (NFI), providing the federal government with the capacity to report on Canada's forests at national and international levels (Gillis 2001). Canada is a large nation, approaching one billion hectares in size, 60% of which is dominated by forested ecosystems composed of a mosaic of land cover types including wetlands, lakes, and variously vegetated areas (Wulder *et al*., 2008a). Excluding other cover types, treed and other wooded lands compose over 40% of the land base in Canada (Natural Resources Canada, 2010).

In Canada, provincial and territorial agencies are vested with stewardship responsibilities over natural resources and allocate licenses for tenure, enabling industrial harvesting activities (Wulder*, Kurz, and Gillis* 2004). Provincial and territorial agencies also implement strategic inventories to inform jurisdictional level planning, which typically use air photo-based forest inventories on an approximate 10-year update cycle (Gillis*, Omule, and Brierly* 2005). Photo-based inventories are typically implemented where there is a capacity for, or interest in, industrial harvesting activities. The jurisdictional inventories are to support strategic decision making, and not required to provide wall-to-wall coverage or for areas that are not applicable (e.g., non-forest areas, parks, remote areas). As a result, in southern Canada, where industrial harvesting activities are more common, extensive inventory datasets are available; conversely, in northern jurisdictions (e.g., Yukon, Northwest Territories) limited areas of these large jurisdictions are systematically represented. The NFI is able to augment the air photo

collection and interpretation undertaken by provincial and territorial agencies to mitigate data acquisition needs, working in partnership to produce the relevant information required by the NFI. The NFI is a sample based inventory using 2 x 2 km photo plots located on a 20 x 20 km grid to produce statistical summaries and reports on Canada's forest resources. In northern Canada, aerial photography is often unavailable in a comprehensive fashion because the industrial extraction of timber resources is limited. As a result, for the establishment of the NFI, information for northern areas of Canada was obtained from the Landsat satellite-based Earth Observation for Sustainable Development of forests (EOSD) project. The circa 2000 EOSD land cover product provides a series of stand attributes (e.g., cover type, volume and biomass) estimated from Landsat-7 Enhanced Thematic Mapper Plus (ETM+) imagery (Wulder *et al*. 2008a). As the update of the NFI photo plots is on-going (Gillis et al. 2005), the use of higher spatial resolution data sources for the characterization of northern areas is also desired. Very High Spatial Resolution (VHSR, < 1 m) commercial satellite imagery, and an associated broad suite of mature image processing approaches, offer significant potential as a data source that can provide relevant forest attributes for the locations and time periods of interest (Falkowski *et al*. 2009).

A detailed review of applications and a framework for implementation of VHSR commercial imagery for estimating a wide range of forest inventory attributes is provided by Falkowski et al. (2009). More detailed investigations of the attribution logic can be found in Mora, Wulder, and White (2010), in which an approach to estimate mean stand height using a regression tree and a series of stand- and crown-level metrics obtained from panchromatic VHSR satellite imagery was developed (R^2 of 0.53, RMSE = 2.84 m). In that study, the authors used an independent sample of photo-interpreted mean stand heights for model calibration and validation, but acknowledged the need to identify more systematic, cost effective, and timely sources of calibration and validation data, particularly for areas where it is difficult to acquire aerial photography. Hence, in this current study, we propose the use of height estimates generated from samples of light detection and ranging (LIDAR) data as an option for calibration and validation of mean stand height estimates generated from VHSR imagery.

Airborne LIDAR has proven to be a robust data source for estimating stand height (Hyyppä *et al*. 2001), particularly for forest management at local scales (Næsset and Økland 2002, Suárez *et al*. 2008). Typically, stand height is estimated using a series of LIDAR metrics regressed against in-situ height measurements (Næsset 2002, Patenaude *et al*. 2004). For example, Holmgren (2004), working in a mixed forest mainly composed of Norway spruce [*Picea abies* (L.) Karst.], Scots pine (*Pinus sylvestris* L.) and birch (*Betula* spp.) in Sweden, estimated Lorey's mean stand height (R^2= 0.99; RMSE = 0.59 m; RMSE-%=3) using regression models based on LIDAR data metrics. Næsset and Oakland (2002) found that LIDAR estimated heights have a similar or better accuracy when compared to corresponding field-based estimates. Studies have demonstrated the capacity of LIDAR data to estimate individual species-specific tree heights with an error rate below 1.0 m when used in a high resolution mode (Persson, Holmgren, and Soderman 2002). The use of LIDAR data has also provided plot-based estimates of maximum and mean tree height with an error below 0.5 m (with full canopy closure conditions) (Næsset 1997, Magnussen and Boudewyn 1998, Næsset and Oakland 2002).

While optical image data, such as Landsat, provides useful information on the horizontal distribution of forest canopy structure, LIDAR provides information on the vertical distribution of forest canopy structure. Hudak *et al*. (2002) explored the synergy

between Landsat-7 ETM+ images and LIDAR data for estimating forest canopy height using aspatial (regression) as well as spatial approaches (kriging). The best method for estimating and mapping canopy height was an integrated model combining spatial and aspatial approaches, by using an ordinary cokriging of stand height residuals obtained from an ordinary least square model (R^2 = 0.88). Optical data sources with a higher spatial resolution have been used to estimate stand height (Peuhkurinen et al. 2008, Mora, Wulder, and White 2010, Chen, Hay, and St-Onge 2011) and could further be integrated with LIDAR for sample based characterizations of height, where the LIDAR data can aid in reducing the bias of height estimates. Wulder and Seemann (2003) proposed a sample-based LIDAR protocol to build stand height regression models that can be applied to support model based attribution over larger areas. Their study, located in the boreal forest of Saskatchewan, Canada, used a model based on an empirical relationship between LIDAR data and forest stand information obtained from Landsat-5 Thematic Mapper (TM) images (R^2 = 0.67, RMSE = 3.3 m, 73% of predicted stand heights were within 6 m of the measured plot heights used for validation).

Based on a subset of inventory attributes (basal area, dominant height, number of trees per hectare), Eid et al. (2004) demonstrated that a LIDAR-based forest inventory provided more precise estimates and was less expensive when compared to a photo interpreted forest inventory. Means et al. (2000) similarly pointed to the potential cost effectiveness of LIDAR and suggested the use of a multi-stage sampling design for the collection of inventory attribute information, whereby an appropriate number of ground measures are collected within the area of LIDAR coverage and are used to build relationships with LIDAR-derived attributes. These relationships, based on this limited ground sample, could then be extended across the entire LIDAR sample, and subsequently, across larger forest areas. Evans, Roberts, and Parker (2006) suggest the use of LIDAR in a double-sampling approach to forest inventory, enabling "credible estimates of forest volume to be achieved with smaller numbers of field plots than would normally be required in a traditional field-only inventory to meet a specific sampling error requirement".

The main objective of this study is to develop and test a sample-based method for using LIDAR data to calibrate and validate VHSR-derived forest stand height estimates. Individual stands (Henley, Wulder, and Falkowski 2009; Wulder et al. 2008b) and tree crowns (Gougeon 1995) were delineated and then used to test a series of metrics, as predictors of stand height, computed at both the tree crown and stand level, as per Mora, Wulder, and White (2010). Four statistical models for estimating mean stand height were tested and the results compared: linear regression, *k*-nearest neighbours (*k*-NN), regression trees, and random forests. LIDAR-derived heights were first calibrated against a sample of ground measured heights. Mean stand heights derived from LIDAR data were then used to calibrate and validate the VHSR height models.

2. Material and methods

2.1. Study area

The study area is located in central British Columbia, west of the town of Quesnel (Figure 1). According to the Ecological Stratification Working Group (1995), the area falls within the Fraser Plateau Ecoregion comprised within the Montane Cordillera Ecozone. Mean annual temperature of the ecoregion is approximately 3°C (-7.5°C in winter and 12.5°C in summer), while the elevation ranges from 750 to 1700 m above sea level. Mean annual precipitation ranges from 250 to 600 mm. Lodgepole pine (*Pinus*

contorta) and Douglas-fir (*Pseudotsuga menziesii*) can be found on drier mid-elevation sites while Engelmann spruce (*Picea engelmannii)* and alpine fir (*Abies lasiocarpa*) are found at subalpine elevations.

Two study sites, each 7000 ha in size, were defined based on the acquired VHSR images spatially corresponding with the LIDAR survey. The study area is dominated by lodgepole pine and previous disturbances, including harvesting (see Site 1 inset in Figure 1) and a recent severe infestation of mountain pine beetle (*Dendroctonus ponderosae* Hopkins) that has resulted in significant pine mortality within the stands. Timber activities (natural and controlled regeneration, clear-cuts, selective logging) occur in the region.

[Figure1 about here]

2.2. Data

LIDAR data were acquired in February 2008 by Terra Remote Sensing (Sidney, British Columbia) using their TRSI Mark II discrete return sensor. The laser data consisted of a north-south trending transect which was approximately 400 m wide and 65 km long. The survey configuration was optimized to achieve a ground return density of 0.7 pulses per m^2 (Table 1). Separation of returns into ground and non-ground classes was completed by the vendor using Terrascan v. 4.006 (Terrasolid, Helsinki, Finland). A 1 m spatial resolution digital elevation model (DEM) was developed from all LIDAR ground returns using a linear interpolation approach.

As the LIDAR data were acquired during winter, the forest floor was covered by snow with an average depth of approximately 0.5 m (σ=0.125 m). The average snow depth was estimated from a rigorous ground survey at nine forested plots (50 m x 50 m plots), with snow depth measured at 36 permanent plot locations spaced 10 m apart within each plot (Varhola *et al.*, 2010). No snow on the branches was observed. The DEM constructed from the LIDAR data was actually a model of the snowpack surface rather than a direct estimate of terrain height or morphology (Coops *et al.* 2009). As a result, vegetation height metrics calculated using the DEM as a ground reference were negatively biased (~ 0.5 m).

[Table 1 about here]

During the summer of 2007, tree surveys were conducted within the same permanent ground plots used for the snow measurement survey. Two of the 36 plots were discarded for the rest of the analysis as they were not within the LIDAR coverage. In each ground plot two or four circular sub-plots having a total area of 100, 200, 400, or 800 m^2 (depending on estimated stem density to capture between 20 and 50 trees per sub-plot) were implemented (Varhola *et al*. 2010). Trees with diameter at breast height (DBH, 1.37 m) greater than 4 cm were counted and their species and defoliation condition were tabulated. Within each circular sub-plot, DBH and height of a subsample of up to 20 trees were measured. Calculated parameters included stems per hectare by species, mean DBH, basal area, and three indicators of plot height (that is, mean height, mean Lorey height, and maximum height). Table 3 provides average forest conditions encountered across the ground plots. The ground plot mean heights were used to calibrate the LIDAR heights (see section 2.7). Two 10 km by 7 km panchromatic (397 - 905 nm) WorldView-1 images with a 0.5 m spatial resolution were acquired for this project (Table 2). To enable

193 the support of a number of research projects, the field data was collected following best
194 practices, in a rigorous manner, with appropriate metadata to have relevance across a
195 number of projects.
196
197
198 *[Table 2 about here]*
199 *[Table 3 about here]*
200
201 ***2.3. LIDAR and VHSR image pre-processing***
202 Plot-level LIDAR height-distribution metrics were calculated using FUSION v. 2.90
203 (McGaughey 2010) for 25 m grid cells. Based on results of previous research
204 demonstrating the stability of first return data (Lim *et al.* 2003), vegetation metrics were
205 processed using only first returns that were greater than 2 m in height. The 2 m height
206 threshold was used to distinguish vegetation hits from ground hits (Nilsson 1996, Næsset
207 2004). Calculated vegetation metrics included the 10, 25, 50, 75, 90, 95, and 99
208 percentiles of the within cell height values (Magnussen and Boudewyn 1998), hereafter
209 noted as HX with X the value of the percentile (e.g., the 90^{th} percentile of height is noted
210 as H90). Also calculated for each cell are the mean, maximum, standard deviation,
211 skewness, kurtosis, and coefficients of variation of vegetation return heights (Næsset and
212 Økland 2002, Hopkinson *et al*. 2006), and several canopy density variables, including the
213 percentage of first returns above the two metre height threshold, and the percentage of
214 first returns above the mean height (Goodwin, Coops, and Culvenor 2006, Hopkinson
215 and Chasmer 2009).
216 Mean stand heights were estimated using a linear regression model (enabling a
217 calibration between the field plots and LIDAR metrics). Model parameters were selected
218 based upon the strength of correlation between the various LIDAR metrics and plot-based
219 height measures. Mean stand height was computed for the delineated stands completely
220 or partially overlaid by the LIDAR coverage, considering only LIDAR data located
221 within a 15 m inner-stand buffer.
222 To process the WorldView-1 images, we first performed a top-of-atmosphere
223 (TOA) spectral radiance conversion following the methods outlined by Krause (2008).
224 The images were then orthorectified using DEMs with a grid resolution of 23 m (Geobase
225 2000). We assessed the precision of the orthorectification procedure using an independent
226 geodetic point dataset (N=10) representative of the topography. We obtained RMSEs of
227 0.64 m and 1.34 m for the image of site 1 and site 2, respectively.
228
229 ***2.4. Stand delineation and classification***
230 Stands were delineated to define objects of homogeneous forest conditions that can then
231 be used to build relationships with the LIDAR height-distribution metrics. For this
232 purpose we used an image segmentation procedure available in Definiens Cognition
233 Network Technology® (DCNT) (Baatz and Schäpe 2000, Definiens Imaging 2004). Prior
234 to segmentation a 3 x 3 pixel median filter was applied to the panchromatic images to
235 avoid over segmentation and reduce convolution of the stand boundaries due to the high
236 spatial resolution of the WorldView-1 images, based on recommendations of Falkowski
237 *et al*. (2009). Following the development of an NFI protocol for segmentation (Henley,
238 Wulder, and Falkowski 2009), a set of initial segmentation parameters has been proposed
239 (scale = 1200, colour = 0.3, and compactness = 0.9) with adjustments to the segmentation
240 parameters undertaken according to the composition of the images (land cover type and

distribution). The resultant segmentation outcomes were reviewed manually to ensure satisfactory grey-level segment homogeneity, i.e., homogeneous within-stand conditions (Wulder *et al.* 2008b).

The delineated segments were then classified with the fuzzy classifier from DCNT software using a basic land-cover stratification so that the forested segments (hereafter referred to as forest, or forested stands) could be isolated for further analysis, and to provide land cover information representative of the entire image area. The classes were selected following NFI and EOSD project standards (Wulder and Nelson 2003) and included: forest, herb, shrub, bryoid, wetland, exposed land, rock, snow-ice (not present), and water.

2.5. Crown delineation

The Individual Tree Crown (ITC) method developed by Gougeon (1995) was applied to the panchromatic images within all the forested stands. The method is based on a valley-following principle (Culvenor, 2003), which in this case requires a lower and an upper grey level value threshold to avoid delineation of non-tree features. The specified range of grey level values determines whether a pixel belongs to a tree crown or the surrounding shadow or understory. The threshold values were adjusted for each image according to the vegetation distribution and structure. Finally, segments with a crown closure less than 10% (N=3) were considered as non-forested (Wulder and Nelson 2003, Natural Resources Canada 2004) and were excluded from the analysis.

2.6. Calculation of VHSR image-based stand-level metrics

Parker, Lowman, and Nadkarni (1995) and Asner, Scurlock, and Hicke (2003) indicate that stand-level estimations based on panchromatic image grey-levels are conditioned by canopy structural attributes such as tree height, crown closure, and stand type. In this study, to capture and relate stand level characteristics to stand height, we first calculated a series of stand-level statistics based on the grey level values of the panchromatic images, including majority, minority, median, mean, standard deviation, range and variety, i.e., the number of unique values of all grey level values in the segment. A second series of stand-level statistics was then calculated based on the ITC output, and include crown closure, mean crown size, and the H25, H50, H75, H90 of crown size distribution.

2.7. Height estimation models

Prior to the computation of stand level metrics, crown objects from the ITC method with abnormal sizes (due to possible clusters of closely located trees or multiple strata of trees, for example) were discarded using the H5 and H95 as lower and upper thresholds, respectively, at the stand level. However, as outlier crowns represented either artefacts or tree clusters that could not be separated, all crown objects were kept to compute crown closure. A stepwise procedure (backward and forward mode) enabled the selection of the best stand metrics to establish the stand height models. The Pearson's correlation analysis of the predictor variables was computed on the forest stand data set overlaid by the LIDAR coverage and used to select the least correlated variables among those considered in this study.

Models to estimate stand height based on VHSR-derived metrics were developed using the data from the delineated stands intersected with LIDAR measurements. The data set was randomly split into a calibration (60% of the stands, i.e., 61 stands) and a validation dataset (40% of the stands, i.e., 36 stands) for all models, i.e., linear regression,

k-NN, regression tree, and random forest models. The random splitting of the dataset was also stratified according to the crown closure, as this parameter was found to influence the calculated metrics. As a result, the entire range of crown closure values was represented in both the calibration and validation datasets. A series of random selections was produced to circumvent any potential bias that could result from a single random selection. The method was implemented so that each forested stand was attributed to the validation data set at least 30 times. In addition, each random splitting was followed by a Multi Response Permutation Procedure (Mielke and Berry 2001) to evaluate the degree to which the calibration and validation data were mutually representative. For each stand, the estimated stand heights were then averaged over the random selections. The *k*-NN, regression tree, and random forest models were built using the metric combinations identified during the stepwise analysis used to guide the regression modelling.

K-NN models were implemented using the R software (R Development Core Team 2005) and the package yaImpute (version 1.0-15) (Crookston and Finley 2008). A series of distance computation methods were tested: Euclidean, Mahalanobis, and an independent component analysis based method (Crookston and Finley 2008). The optimal number of neighbours to consider was estimated over the computation of one thousand random data set divisions into calibration and validation datasets followed by the modelling of height with values of *k* ranging from 1 to 30. From these tests, we selected the optimal value of *k*.

The linear regression models were established using the R software and the package stats (version 2.13.1). The regression tree method was established as proposed in Mora, Wulder, and White (2010), using a 10-fold cross validation procedure followed by a tree pruning stage based on best practices (McLachlan, Do, and Ambroise 2004). Regression trees were implemented using the R software and the package tree (version 1.0-28) (Ripley 2009). The random forest method was implemented using the R software and the package randomForest (version 4.6-2) (Breiman 2001).

3. Results

3.1. Stand identification and stand metrics

A total of 2245 segments were delineated over the two images, of which 1520 were subsequently classified as forest stands, including 111 stands intersected by the LIDAR transect that became the focus on this study. In addition, the analysis of the stand crown closure values led to the identification and removal of 9 outlier stands. These outliers represent stands for which the boundaries were not accurately delineated, or included water features and/or roads. The resulting dataset had 97 forested stands with crown closure values ranging from 25% to 62% with a mean of 47%. Table 4 summarizes stand metrics obtained from the grey level values and the delineated crowns.

[Table 4 about here]

3.2. Stand height estimation

First, LIDAR heights were calibrated using ground plot heights and a linear regression model. Following independent variable data selection, a univariate model using H90 was the most successful model (R^2 =0.91, SE = 2.98 m (SE-%=26)). Among the several metrics selected, combinations between the median grey level value in the segment (median_S) with the H25 and the H90 of the crown area distribution (H25_C and H90_C, respectively) provided the best models (Table 5). The residuals of both linear regression

models had a normal distribution (p = 0.83 for both). Homoscedasticity was verified for the 2-metric model (median_S and H90_C; p = 0.03) and was close to be verified for the 3-metric model (median_S, H25_C, and H90_C; p = 0.07) with α = 0.05. A t-test showed no significant differences between LIDAR and estimated mean stand heights (p >= 0.95) for both models. Table 6 presents the values of the Pearson's correlation analysis between these three metrics. Figure 2a shows the scatter plot of the LIDAR heights and those estimated by the best 2-metric linear regression model.

[Table 5 about here]
[Table 6 about here]

Regression trees were tested with the two sets of predictor metrics (Table 7) previously identified. Both tests provided lower coefficients of determination and lower performance in estimating stand heights compared to the linear regression models. Figure 2b shows the scatter plot between the LIDAR heights and those estimated by the 2-metric model.

[Table 7 about here]

The random forest method was tested for the same metric combinations previously selected and provided better results than the regression tree method, but did not outperform the linear regression model. The 3-metric model provided similar results as those obtained with the 2-metric linear regression model. Table 8 presents the results obtained for these tests. Figure 2c shows the scatter plot between the LIDAR heights and those estimated by the 3-metric model.

[Table 8 about here]

We determined that the best number of neighbours was 4 for the k-NN method. The two-metric model provided the best R^2 and RMSE when used in conjunction with an independent component analysis (ICA)-based distance calculation method (Table 9). However, the number of metrics and the method selected to compute the distances did not significantly change the performance of the model, providing RMSEs with a limited range from 2.3 m to 2.6 m. Figure 2d shows the scatter plot of the LIDAR heights versus those estimated by the 2-metric model. The evaluation of the residuals for the best model (k-NN) according to the LIDAR stand heights shows little bias overall (Figure 3), with a positive bias evident for shorter stands and a negative bias for the taller stands. Figure 4 presents the evolution of the residuals of the best model according to the within-stand LIDAR height variation and reveals no link between these two statistics, indicating that a correct level of image segmentation was performed.

[Table 9 about here]
[Figure 2 about here]
[Figure 3 about here]
[Figure 4 about here]

We calculated the standard deviation of the stand height estimates across the random selections for each stand. Figure 5 summarizes the calculations providing the

385 minimum, maximum, and mean standard deviation values for stand height in the best
386 performing version of a given model.
387
388 *[Figure 5 about here]*
389
390 **4. Discussion**
391 Imputation methods typically provide lower performance than regression methods
392 because they are not designed to minimize least-square errors (Stage and Crookston
393 2007). However, the single imputation method (*k*-NN method, *k* = 4, ICA-based
394 distance), provided the best model fit statistics in this study (R^2 = 0.69, RMSE = 2.3 m,
395 RMSE-%=21) over the regression methods when considering the median_S and the
396 H90_C as predictors. The ICA method was developed to compute distances in a projected
397 space defined by statistically independent components (Hyvarinen and Oja 2000)
398 assuming non-Gaussian distributions. Therefore, this distance calculation method allows
399 greater options in the application of the *k*-NN over heterogeneous datasets, that is,
400 varying stand parameter distributions. Note that the *k*-NN method has previously
401 demonstrated some potential in canopy height modelling when associated with airborne
402 LIDAR and satellite imagery data in a LIDAR-plot based framework (McInerney *et al*.
403 2010). The choice of the distance calculation method among the three that were tested did
404 not drastically influence the R^2 and RMSE values (Table 9).
405 Despite a lower R^2 (0.59), the 2-metric linear regression model was considered for
406 comparison rather than the 3-metric model (R^2 = 0.64), as some of the mean variance
407 inflation factor (VIF) values of the latter were higher and the correlation between the H25
408 and the H90_C was 0.88 (Table 6). The 2-metric linear regression model provided
409 acceptable stand height accuracy (SE = 2.6 m (SE-%=21)). Both R^2 and SE improved
410 compared to the study from Mora, Wulder, and White (2010) where stand height was
411 modelled with regression trees applied to similar VHSR-derived metrics, but which were
412 calibrated and validated with photo interpreted heights. Both random forest and
413 regression tree models performed weakly relative to the linear regression and *k*-NN
414 models, with R^2 values equal or lower than 0.59, and RMSEs ranging from 2.7 m for the
415 best random forest model to more than 4 m for the regression tree models.
416 The study of the variation of the stand height estimates showed reasonably low
417 variations with mean standard deviations (across the stands) for each model below 1 m,
418 except for the regression tree model (Table 10). The maximum standard deviation was
419 below 2 m, except for the regression tree model (4.05 m). Regression trees and random
420 forests operate recursive data partitioning that aims at improving cluster homogeneity
421 while the k-NN method realizes an imputation process. These three models produce a
422 mean response that is constrained to the range of sample observations and requires a
423 representative sample dataset to produce highly effective estimations. The random forests
424 model provides a mean response that is based on averaging of the results from multiple
425 trees built internally. Therefore, it would be expected that the random forests model
426 would provide more consistent results compared to regression trees, as was observed in
427 this study (Table 10). The capacity of a *k*-NN method to provide consistent results will
428 depend notably on the number of neighbours (*k*) considered (*k*=4 in this study). In
429 contrast, linear regression models tend to provide the most consistent estimates of all the
430 methods examined in this study. This is due to the fact that the linear regression enables a
431 better fit to the data, with interpolations made between discontinuous observations and
432 beyond the range of observations.

All forest stands considered in the study area were classified as coniferous according to the provincial forest inventory, with no mixed stands found within the LIDAR transect. Therefore, it was not necessary to build models distinguishing stand types. However, as might be expected, some smaller deciduous trees patches were visually identified over the study region. The LIDAR data were acquired during the winter of 2008 and the VHSR images during summer and early fall of 2009; therefore, the LIDAR data were acquired under leaf-off deciduous tree conditions, while the VHSR images were acquired during leaf-on conditions. Such conditions could have resulted in marginal discrepancies between the VHSR grey level values, the crown area statistics, and the LIDAR returns. In addition, pine beetle infestations have been reported over the study region (Bater *et al*. 2010; Varhola *et al*. 2010). The attacks may have biased some stand metric estimations as the infestation can have an impact on the crown reflective properties (grey stage) when observed in the panchromatic spectral range of the WorldView-1 sensor, as well as on the LIDAR returns (Coops *et al*. 2009).

The best overall model in this study was the single imputation method (*k*-NN method, $k = 4$, ICA-based distance) using median_S and H90_C with an RMSE of 2.3 m. To provide some context for this result, it is useful to examine the literature; however, few studies have used LIDAR data to calibrate estimates of mean stand height from optical remotely sensed data in similar forest environments (e.g., Hudak et al., 2002; Wulder and Seemann, 2003). Of these, even fewer have reported RMSE errors, which are necessary for understanding the magnitude of the error associated with a given approach and data type. Wulder and Seemann (2003) integrated Landsat-5 TM data and LIDAR samples to estimate mean stand height with an RMSE of 3.3 m. Studies that use VHSR imagery exclusively have produced results similar to those of Wulder and Seemann (2003). For example, Peuhkurinen et al. (2008) used a variety of IKONOS spectral features in a k-most similar neighbor (K-MSN) approach to estimate mean stand height with an RMSE of 3.1 m. Similarly, Chen, Hay, and St-Onge. (2011) used an object-based approach with pan-sharpened QuickBird data to estimate mean stand height with an RMSE of 3.37 m. In an approach similar to that described herein (without LIDAR calibration), Mora, Wulder, and White (2010) used QuickBird data and a regression tree approach to estimate mean stand height with an RMSE of 2.84 m. Thus, the methods developed herein are capable of providing estimates of mean stand height that improve upon estimates generated without the benefit of lidar calibration.

Our objective with this work was to describe a VHSR satellite-based method enabling the estimation of mean stand height, which was established using LIDAR data calibrated with field data. Similar multi-stage studies were carried out over forested environments with medium spatial resolution imagery (Landsat) (Duncanson, Niemann, and Wulder 2010, Li *et al*. 2011) and high spatial resolution imagery (QuickBird) (Hilker, Wulder, and Coops 2008), with the Geoscience Laser Altimeter System instrument (onboard the now defunct ICESat (Ice, Cloud, and land Elevation satellite)), and airborne LIDAR respectively. The models based on *k*-NN, linear regressions, and random forests provided acceptable accuracies compared to, for example, the forest inventory standards in British Columbia where the quality control of photo interpreted heights specifies an error range of ± 3 m (Ministry of Forests and Range 2009). However, all the models used in this study inherit qualities from the regression model built to compute the stand heights from the LIDAR and ground observations (SE = 2.98 m (SE-%=26)). This gain in accuracy may result from the loss of variability in the fitted height values. Whatever the method used to build the stand height model, metrics from both the

stand grey level values and crown metrics were required to get satisfactory results and model reliability. However, the current study and the previously mentioned literature provide guidance to facilitate the implementation of the methodology and its partial automation.

The current study demonstrates the capacity of using LIDAR data to calibrate and validate stand height estimates generated from VHSR imagery. For a large area, such as Canada's northern forests, the cost of collecting wall-to-wall LIDAR or VHSR imagery is prohibitive; however, the ability to collect samples of both data types and integrate them in a plot-based framework allows for the robust estimation of stand heights in areas with no other available information. Hilker *et al.* (2008) found no statistical difference between stand heights estimated from a complete wall-to-wall LIDAR coverage and those estimated from a single 400 m wide LIDAR transect, demonstrating that a sample-based approach is both logistically feasible and financially prudent.

The CFS conducted a LIDAR survey across Canada during the summer of 2010, resulting in a series of transects totalling over 25,000 km in length, specified for a minimum swath width of 500 m and a minimum of 3 points per m^2, with FUSION metrics produced as in this study using a 25 x 25 m cell size (Wulder *et al*., in prep). NFI photo plots intersecting the LIDAR swaths could be considered as appropriate study sites to strengthen and validate the LIDAR-plot based methodology established in this study. We also envisage the application of LIDAR-plot developed models more widely to NFI photo plot locations using generalized regionally appropriate models (ecozone level) to preclude the need for LIDAR over all northern NFI photo plot locations. The number of sample plots covered by both VHSR and LIDAR data should be sufficient enough to capture the full range of forest conditions (stand type, height and crown size distribution) occurring in the region, enabling the establishment of a representative and reliable stand height model. To ensure the calculations of consistent and reliable stand metrics, we recommend acquiring LIDAR data and VHSR imagery during summer time, and when possible during the same period of time. In addition, when atmospheric conditions and image archive allow, VHSR image acquisition parameters (e.g., sun angle, view angle) should be consistent across the set of images used to build a given model to ensure consistency of the stand metric calculations (Wulder *et al*. 2008c).

5. Conclusion

In this study, we investigated the potential of four statistical methods to model mean stand height from VHSR panchromatic and tree crown metrics using a multi-stage LIDAR-plot based method for model calibration and validation. We compared the model estimated heights to those generated from the airborne LIDAR. The study showed that the *k*-NN method was able to produce the best model ($R^2 = 0.69$, RMSE = 2.3 m, RMSE-%=21) as a result of variance explained and residual analysis. Based upon the R^2 value and the low RMSE, operational utility of the approach and outcomes is provided, while typical cautions for use of empirical equations should be observed. Compared to our previous study (Mora, Wulder, and White 2010), this current work also demonstrated the need to combine metrics computed at stand and tree crown levels to obtain the best results. This work demonstrated a parsimonious method that minimizes ground measurements to a limited sample required for the calibration of LIDAR heights. In addition, the study provided insights on the image segmentation procedure defined, supporting previous research, and providing insights towards operationalization. For instance, the research demonstrated that the selected segmentation parameters provided

low within-stand LIDAR height variance. Overall, this study demonstrates the potential of VHSR panchromatic imagery for estimating stand height over remote areas when supported by LIDAR-plots to provide calibration (and subsequent validation). The proposed methodology can be adapted to enable the direct estimation of other stand attribute estimates such as volume and biomass.

6. Acknowledgements

This research was undertaken as part of the "EcoMonitor: Northern Ecosystem Climate Change Monitoring" project jointly funded by the Canadian Space Agency (CSA) Government Related Initiatives Program (GRIP) and the Canadian Forest Service (CFS) of Natural Resources Canada. We also wish to thank Dr. Gordon Frazer for his helpful insights and discussions allowing for an improvement to the methods employed in this study. We also thank the reviewers of an initial version of this manuscript for their constructive and insightful comments.

7. References

NATURAL RESOURCES CANADA, 2010, *The state of Canada's forests 2010.* Canadian Forest Service, Natural Resources Canada. Ottawa, ON, Canada.

ASNER, G.P., SCURLOCK, J.M.O., and HICKE, J.A., 2003, Global synthesis of leaf area index observations: Implications for ecological and remote sensing studies. *Global Ecology and Biogeography*, **12**, pp. 191−205.

BAATZ, M., and SCHÄPE, M., 2000, Multiresolution segmentation: An optimization approach for high quality multi-scale image segmentation. In *Angewandte Geographische Informationsverarbeitung XII*. *Beitrage zum AGIT- Symposium Salzburg 2000*, Strobl, J. and Blaschke, T. (Eds.), pp.12–23 (Karhlsruhe: Herbert Wichmann Verlag).

BATER, C.W., WULDER, M.A., WHITE, J.C., and COOPS, N.C., 2010, Integration of LIDAR and Digital Aerial Imagery for Detailed Estimates of Lodgepole Pine (Pinus contorta) Volume Killed by Mountain Pine Beetle (Dendroctonus ponderosae). *Journal of Forestry*, **108**, pp. 111−119.

BOUDEWYN, P., SONG, X., MAGNUSSEN, S., and GILLIS, M.D., 2007, *Model-based, volume-to-biomass conversion for forested and vegetated land in Canada*. Victoria, British Columbia: Canadian Forest Service, Pacific Forestry Centre BC-X-411.

BREIMAN, L. 2001, Random Forests, *Machine Learning,* **45**, pp. 5−32.

CHEN, G., HAY, G.J., ST-ONGE, B., 2011, A GEOBIA framework to estimate forest parameters from lidar transects, Quickbird imagery, and machine learning: A case study in Quebec, Canada. *International Journal of Applied Earth Observation and Geoinformation,* **15**, pp. 28–37.

COOPS, N.C., VARHOLA, A., BATER, C.W., TETI, P., BOON, S., GOODWIN, N., and WEILER, M., 2009, Assessing differences in tree and stand structure following beetle infestation using lidar data. *Canadian Journal of Remote Sensing*, **35,** pp**.** 497−508.

CROOKSTON, N.L. and FINLEY. A.O., 2008, yaImpute: An R Package for kNN Imputation. *Journal of Statistical Software*, **23,** 16 pp.

575 CULVENOR, D.S., 2003, Survey of techniques for extracting individual tree information
576 from high spatial resolution imagery. In *Remote sensing of forest environments:*
577 *concepts and case studies*. M.A. Wulder and S.E. Franklin (Eds.), pp. 225–279
578 (Boston: Kluwer Academic Publishers).
579 DEFINIENS IMAGING, 2004, *eCognition elements: User guide 4*. Germany: München,
580 71 pp.

581 DUNCANSON, L. I., NIEMANN, K. O., and WULDER, M. A., 2010, Integration of
582 GLAS and Landsat TM data for aboveground biomass estimation. Canadian Journal
583 of Remote Sensing, **36**, pp. 129-141.

584 ECOLOGICAL STRATIFICATION WORKING GROUP, 1995, *A National ecological*
585 *framework for Canada*. Agriculture and Agri-Food Canada, Research Branch,
586 Centre for Land and Biological Resources Research and Environment Canada, State
587 of the Environment Directorate, Ecozone Analysis Branch, Ottawa/Hull.

588 EVANS, D.L., ROBERTS, S.D., and PARKER, R.C., 2006, LiDAR – A new tool for
589 forest measurements. *The Forestry Chronicle,* **82**, pp. 211-218.
590 FALKOWSKI, M.J., WULDER, M.A., WHITE, J.C., and GILLIS, M.D., 2009,
591 Supporting large-area, sample-based forest inventories with very high spatial
592 resolution satellite imagery. *Progress in Physical Geography*, **33**, pp. 403–423.
593 GEOBASE, 2000, Canadian Digital Elevation Data, Level 1 Product Specifications.
594 Edition 3.0 (2007-06-01). Government of Canada, Natural Resources Canada, Earth
595 Sciences Sector, Centre for Topographic Information. Sherbrooke, Quebec, Canada.
596 Available online at:
597 http://www.geobase.ca/doc/specs/pdf/GeoBase_product_specs_CDED1_3_0.pdf
598 (accessed 1 April 2011).
599 GILLIS, M.D., 2001, Canada's National Forest Inventory (responding to current
600 information needs). *Environmental Monitoring and Assessment*, **67**, pp. 121-129.
601 GILLIS, M.D., OMULE, A.Y., and BRIERLEY, T., 2005, Monitoring Canada's forests:
602 The National Forest Inventory. *The Forestry Chronicle*, **81**, pp. 214−221.
603 GOODWIN, N.R., COOPS, N.C., CULVENOR, D.S., 2006, Assessment of forest
604 structure with airborne LIDAR and the effects of platform altitude. *Remote Sensing*
605 *of Environment*, **103**, pp. 140–152.
606 GOUGEON, F.A., 1995, crown-following approach to the automatic delineation of
607 individual tree crowns in high spatial resolution aerial images. *Canadian Journal of*
608 *Remote Sensing*, **21**, pp. 274−284.
609 HENLEY, M.J., WULDER, M.A., and FALKOWSKI, M.J., 2009, *EcoMonitor*
610 *segmentation methodology*, Version 2.0. Canadian Forest Service. Victoria, British
611 Columbia: Pacific Forestry Centre.
612 HILKER, T., WULDER, M. A., and COOPS, N. C. 2008, Update of Forest Inventory
613 Data with Lidar and High Spatial Resolution Satellite imagery. *Canadian Journal*
614 *of Remote Sensing*, **34**, pp. 5-12.
615 HOLMGREN, J., 2004, Prediction of Tree Height, Basal Area and Stem Volume in
616 Forest Stands Using Airborne Laser Scanning. *Scandinavian Journal of Forest*
617 *Research*, **19**, pp. 543−553.
618 HOPKINSON, C., CHASMER, L., 2009, Testing LiDAR models of fractional cover
619 across multiple forest ecozones. *Remote Sensing of Environment*, **113**, pp. 275–288.

620 HOPKINSON, C., CHASMER, L., LIM, K., TREITZ, P., CREED, I., 2006, Towards a
621 universal lidar canopy height indicator. *Canadian Journal of Remote Sensing*, **32**,
622 pp. 139–152.
623 HUDAK, A.T., LEFSKY, M.A., COHEN, W.B., and BERTERRETCHE, M., 2002,
624 Integration of lidar and landsat TM+ data for estimating and mapping forest canopy
625 height. *Remote Sensing of Environment*, **82**, pp. 397−416.
626 HYVARINEN, A., and OJA, E., 2000, Independent Component Analysis. *Neural*
627 *Networks*, **13**, pp. 411–430.
628 HYYPPÄ, J., KELLE, O., LEHIKOINEN, M. and INKINEN, M., 2001, A segmentation-
629 based method to retrieve stem volume estimates from 3-D tree height models
630 produced by laser scanners. *Transactions on Geoscience and Remote Sensing*, **39**,
631 pp. 969–975.
632 KRAUSE, K.S. 2008, WorldView-1 pre and post-launch radiometric calibration and
633 early on-orbit characterization. *Proceedings of SPIE Earth Observing Systems XIII*,
634 **7081**.

635 LI, A., HUANG, C., SUN, G., SHI, H., TONEY, C., ZHU, Z., ROLLINS, M. G.,
636 GOWARD, S. N., and MASEK, J. G., 2011, Modeling the height of young forests
637 regenerating from recent disturbances in Mississippi using Landsat and ICESat data.
638 *Remote Sensing of Environment*, **115**, pp. 1837-1849. Elsevier Inc. doi:
639 10.1016/j.rse.2011.03.001.

640 LIM, K., TREITZ, P., WULDER, M., ST-ONGE, B., and FLOOD, M., 2003, Lidar
641 remote sensing of forest structure. *Progress in Physical Geography*, **27**, pp. 88-106.
642 MAGNUSSEN, S., BOUDEWYN, P., 1998, Derivations of stand heights from airborne
643 laser scanner data with canopy-based quantile estimators. *Canadian Journal of*
644 *Forest Research*, **28**, pp. 1016−1031.
645 MCGAUGHEY, R.J., 2010, FUSION/LDV: *Software for LIDAR data analysis and*
646 *Visualization,* Version 2.90. Pacific Northwest Research Station, Forest Service,
647 United States Department of Agriculture.
648 MCINERNEY, D.O., SUAREZ-MINGUEZ, J., VALBUENA, R., and NIEUWENHUIS,
649 M., 2010, Forest canopy height retrieval using Lidar data, medium-resolution
650 satellite imagery and kNN estimation in Aberfoyle, Scotland. *Forestry*, **83**, pp.
651 195−206.
652 MCLACHLAN, G.J., DO, K.A., and AMBROISE, C. (Eds.), 2004, *Analyzing*
653 *microarray gene expression data*, 320 pp. (New Jersey: John Wiley and Sons).
654 MEANS, J.; ACKER, S.; FITT, B.; RENSLOW, M.; EMERSON, L., AND HENDRIX,
655 C. 2000. Predicting forest stand characteristics with airborne scanning lidar.
656 *Photogrammetric Engineering & Remote Sensing*. 66(11):1367-1371.
657 MIELKE, P.W. Jr., and BERRY, K.J. (Ed.), 2001, *Permutation methods: A distance*
658 *function approach*, 352 pp. (New York: Springer-Verlag).
659 MINISTRY OF FORESTS AND RANGE, 2009, Vegetation Resources Inventory: Photo
660 Interpretation Quality Assurance Procedures and Standards, Version 3.2.Victoria,
661 British Columbia: Forest Analysis and Inventory Branch. Available online at:
662 http://www.for.gov.bc.ca/hts/vri/standards/index.html#photo (accessed 1 April
663 2011).
664 MORA, B., WULDER, M.A., and WHITE, J.C., 2010, Segment-constrained regression
665 tree estimation of forest stand height from very high spatial resolution panchromatic

imagery over a boreal environment. *Remote Sensing of Environment*, **114**, pp. 2474–2484.

NÆSSET, E. 1997. Determination of mean tree height of forest stands using airborne laser scanner data. ISPRS Journal of Photogrammetry and Remote Sensing, 52(2), 49-56.

NÆSSET, E., 2002, Predicting forest stand characteristics with airborne scanning laser using a practical two-stage procedure and field data. *Remote Sensing of Environment*, **80**, pp. 88−99.

NÆSSET, E. and ØKLAND, T., 2002, Estimating tree height and tree crown properties using airborne scanning laser in a boreal nature reserve. *Remote Sensing of Environment*, **79**, pp. 105–115.

NÆSSET, E., 2004, Practical large-scale forest stand inventory using a small-footprint airborne scanning laser. *Scandinavian Journal of Forest Research*, **19**, pp. 164-179.

NATURAL RESOURCES CANADA., 2004, *Canada's National Forest Inventory: Photo plot guidelines*, Version 1.1. Internal Design Document. Victoria, British Columbia: Canadian Forest Service, Pacific Forestry Centre.

NILSSON, M., 1996 Estimation of tree heights and stand volume using an airborne lidar system. *Remote Sensing of Environment,* **56**, pp. 1-7.

PATENAUDE, G., HILL, R., MILNE, R., GAVEAU, D., BRIGGS, B., and DAWSON, T., 2004, Quantifying forest above ground carbon content using LiDAR remote sensing. *Remote Sensing of Environment*, **93**, pp. 368−380.

PARKER, G.G., LOWMAN, M., and NADKARNI, N., 1995, Structure and microclimate of forest canopies. In *Forest canopies: A review of research on a biological frontier,* M. D. Lowman, and N. M. Nadkarni (Eds.)*,* pp. 73−106 (San Diego: Academic Press).

PERSSON, Å., HOLMGREN, J., and SODERMAN, U., 2002, Detecting and Measuring Individual Trees Using an Airborne Laser Scanner. *Photogrammetric Engineering & Remote Sensing*, **68**, pp. 925-932.

PEUHKURINEN, J., MALTAMO, M., VESA, L., and PACKALÉN, P. 2008, Estimation of Forest Stand Characteristics Using Spectral Histograms Derived from an Ikonos Satellite Image. *Photogrammetric Engineering & Remote Sensing*, **74**, pp. 1335-1341.

R DEVELOPMENT CORE TEAM, 2005, R: A language and environment for statistical computing. Vienna, Austria: R Foundation for Statistical Computing. Available online at: http://www.R-project.org (accessed 1 April 2011).

RIPLEY, B., 2009, tree: Classification and regression trees. R package version 1.0-27. Available online at: http://CRAN.R-project.org/package=tree (accessed 1 April 2011).

STAGE, A.R., and CROOKSTON, N., 2007, Partitioning Error Components for Accuracy-Assessment of Near-Neighbor Methods of Imputation. *Forest Science*, **53**, pp. 62−72.

SUÁREZ, J.C., GARCIA, R., GARDINER, B. and PATENAUDE, G., 2008, The estimation of wind risk in forest stands using Airborne Laser Scanning (ALS). *Journal of Forest Planning*, **13**, pp. 165–185.

VARHOLA, A., COOPS, N.C., BATER, C.W., TETI, P., BOON, S., and WEILER, M., 2010, The influence of ground- and LiDAR-derived forest structure metrics on snow accumulation and ablation in disturbed forests. *Canadian Journal of Forest Research*, **40**, pp. 812−821.

WULDER, M.A., J.C. WHITE, C.W. BATER, N.C. COOPS, C. HOPKINSON, AND G. CHEN. (2012). LIDAR PLOTS—A NEW LARGE-AREA DATA COLLECTION OPTION: CONTEXT, CONCEPTS, AND CASE STUDY. CANADIAN JOURNAL OF REMOTE SENSING. VOL. 38, NO. 05, PP. 600-618. (DOI: HTTP://DX.DOI.ORG/10.5589/M12-049) WULDER, M.A. and SEEMANN, D., 2003, Forest inventory height update through the integration of lidar data with segmented Landsat imagery. *Canadian Journal of Remote Sensing*, **29**, pp. 536−543.

WULDER, M. and NELSON, T., 2003, EOSD Land Cover Classification Legend Report - Version 2, Natural Resources Canada, Canadian Forest Service, 83 pp.

WULDER, M.A., KURZ, W., and GILLIS, M., 2004, National level forest monitoring and modelling in Canada. *Progress in Planning*, **61**, pp. 365−81.

WULDER, M.A., WHITE, J.C., CRANNY, M., HALL, R.J., LUTHER, J.E., BEAUDOIN, A., GOODENOUGH, D.G., and DECHKA, J.A., 2008a, Monitoring Canada's forests. Part 1: Completion of the EOSD Land Cover Project. *Canadian Journal of Remote Sensing*, **34**, pp. 549−562.

WULDER, M.A., WHITE, J.C., HAY, G.J., and CASTILLA, G., 2008b, Towards automated segmentation of forest inventory polygons on high spatial resolution satellite imagery. *The Forestry Chronicle*, **84**, pp. 221−230.

WULDER, M.A., ORTLEPP, S.M., WHITE, J.C., and COOPS, N.C., 2008c, Impact of Sun-Surface-Sensor Geometry Upon Multitemporal High Spatial Resolution Satellite Imagery. *Canadian Journal of Remote Sensing*, **34**, pp. 455−461.

List of Tables

List of Figures

Table 1. Summary of LIDAR survey flight and sensor parameters.

Attribute	Value
Platform	Bell 206 Jet Ranger helicopter
Flying height (m)	800
Sensor	TRSI Mark II
Number of returns	Two, first and last
Laser wavelength (nm)	1,064
Pulse repetition frequency (kHz)	50
Maximum scan angle (degrees)	±15
Beam divergence angle (mrad)	0.5
Footprint diameter (m)	0.4
Swath width (m)	400
Nominal ground return density (returns/m^2)	0.7

Table 2. WorldView-1 image acquisition parameters.

	Size (ha)	Plot center coordinates		Acquisition date	Solar azimuth (degrees)	Solar elevation (degrees)	Satellite azimuth (degrees)	Satellite elevation (degrees)	Off-nadir view angle (degrees)	In-track view angle (degrees)	Cross-track view angle (degrees)
		Latitude	longitude								
Site 1	7000	53°03’01’’	122°56’53’’	07/25/2009	164.6	55.9	293.8	71.9	16.8	2.9	-16.6
Site 2	7000	52°36’53’’	122°55’59’’	09/23/2009	170.4	36.8	187.0	85.9	3.6	-3.6	0.3

Table 3. Average biophysical conditions encountered across the ground plots.

	Terrain elevation (m)	dbh (cm)	Basal area (m^2/ha)	Mean height (m)	Maximum height (m)	Conifer (%)
Mean	1110	13	31	11	18	99
Standard deviation	140	6	17	4	7	1

Table 4. Mean and standard deviation of image grey level values and tree crowns for segment level metrics used as inputs to the models.

Source Data	Metric	Mean	Standard Deviation
QuickBird TOA spectral radiance values	minority ($W.sr^{-1}.m^{-2}.\mu m^{-1}$)	1.38	1.14
	majority ($W.sr^{-1}.m^{-2}.\mu m^{-1}$)	1.45	.38
	median ($W.sr^{-1}.m^{-2}.\mu m^{-1}$)	1.58	.30
	mean ($W.sr^{-1}.m^{-2}.\mu m^{-1}$)	1.64	.27
	standard deviation ($W.sr^{-1}.m^{-2}.\mu m^{-1}$)	.43	.08
	range ($W.sr^{-1}.m^{-2}.\mu m^{-1}$)	3.20	.46
	variety ($W.sr^{-1}.m^{-2}.\mu m^{-1}$)	2.94	.38
Individual ITC-defined tree crowns	crown closure (%)	45	9
	mean crown size (m^2)	6	1
	H25 of crown size distribution (m^2)	3	0.5
	H50 of crown size distribution (m^2)	5	0.9
	H75 of crown size distribution (m^2)	8	2
	H90 of crown size distribution (m^2)	12	3

Table 5. Results from the best linear regression models with mean VIF: variance inflation factor, and SE: standard error.

Metrics	mean VIF	R^2	SE (m)
median_S	1.7	0.64	2.5
H25_C	4.8		
H90_C	6.1		
median_S	1.2	0.59	2.7
H90_C	1.2		

Table 6. Pearson's correlation table of the best metrics.

	median_S	H25_C	H90_C
median_S	/	0.62	0.47
H25_C		/	0.88

Table 7 Error! Reference source not found.**. Results from the best regression tree models.**

Metrics	R^2	RMSE (m)
median_S H25_C H90_C	0.54	4.3
median_S H90_C	0.55	4.2

Table 8. Results from the best random forest models.

Metrics	R^2	RMSE (m)
median_S H25_C H90_C	0.59	2.7
median_S H90_C	0.55	2.8

Table 9. Results for the best K-NN models, with RMSE.

Metrics	Distance	R^2	RMSE (m)
median_S, H25_C, H90_C	euclidean	0.67	2.4
	mahalanobis	0.63	2.6
	ICA-based	0.64	2.5
median_S, H90_C	euclidean	0.65	2.5
	mahalanobis	0.68	2.4
	ICA-based	0.69	2.3

Figure 1. Study area located in British Columbia, Canada. The WorldView-1 image locations are also noted.

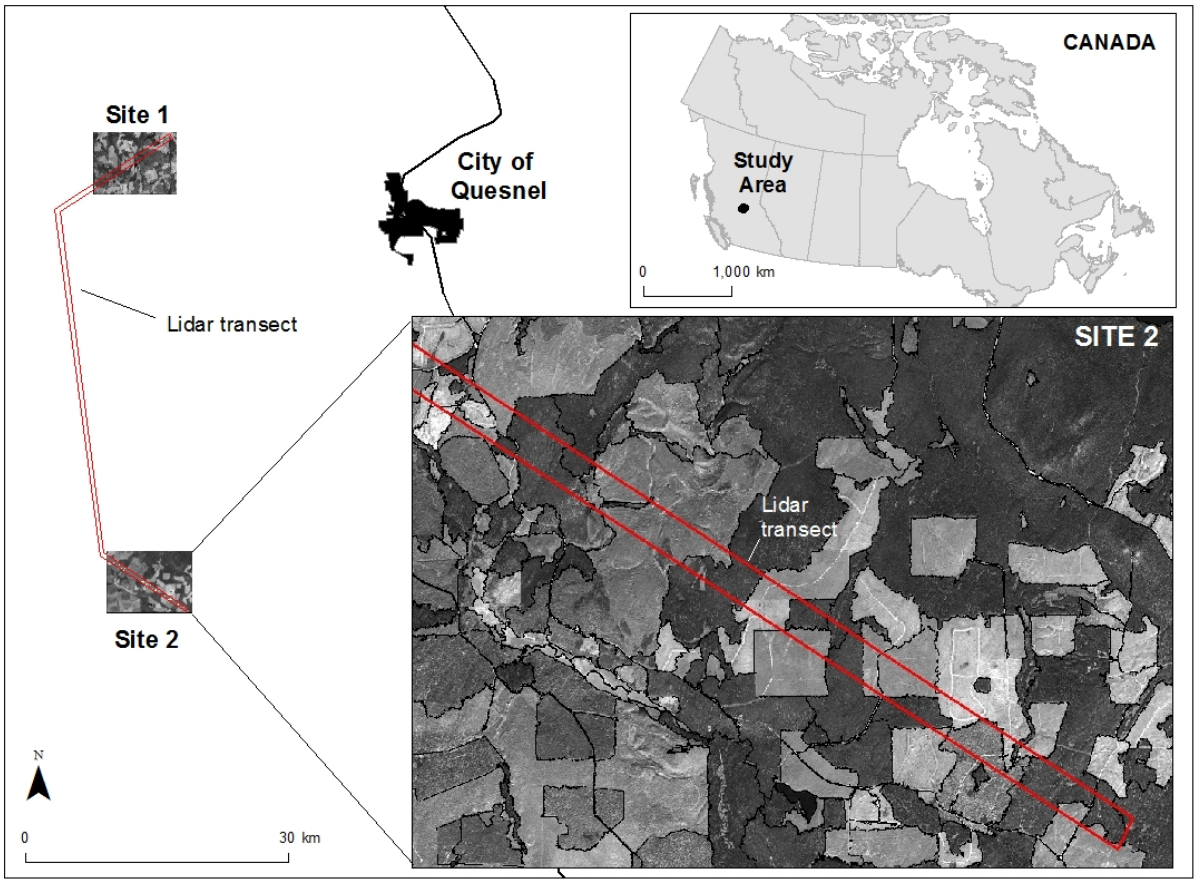

Figure 2. Scatter plots of the LIDAR heights versus best estimated heights from a) linear regression b) regression trees c) random forests, and d) KNN models.

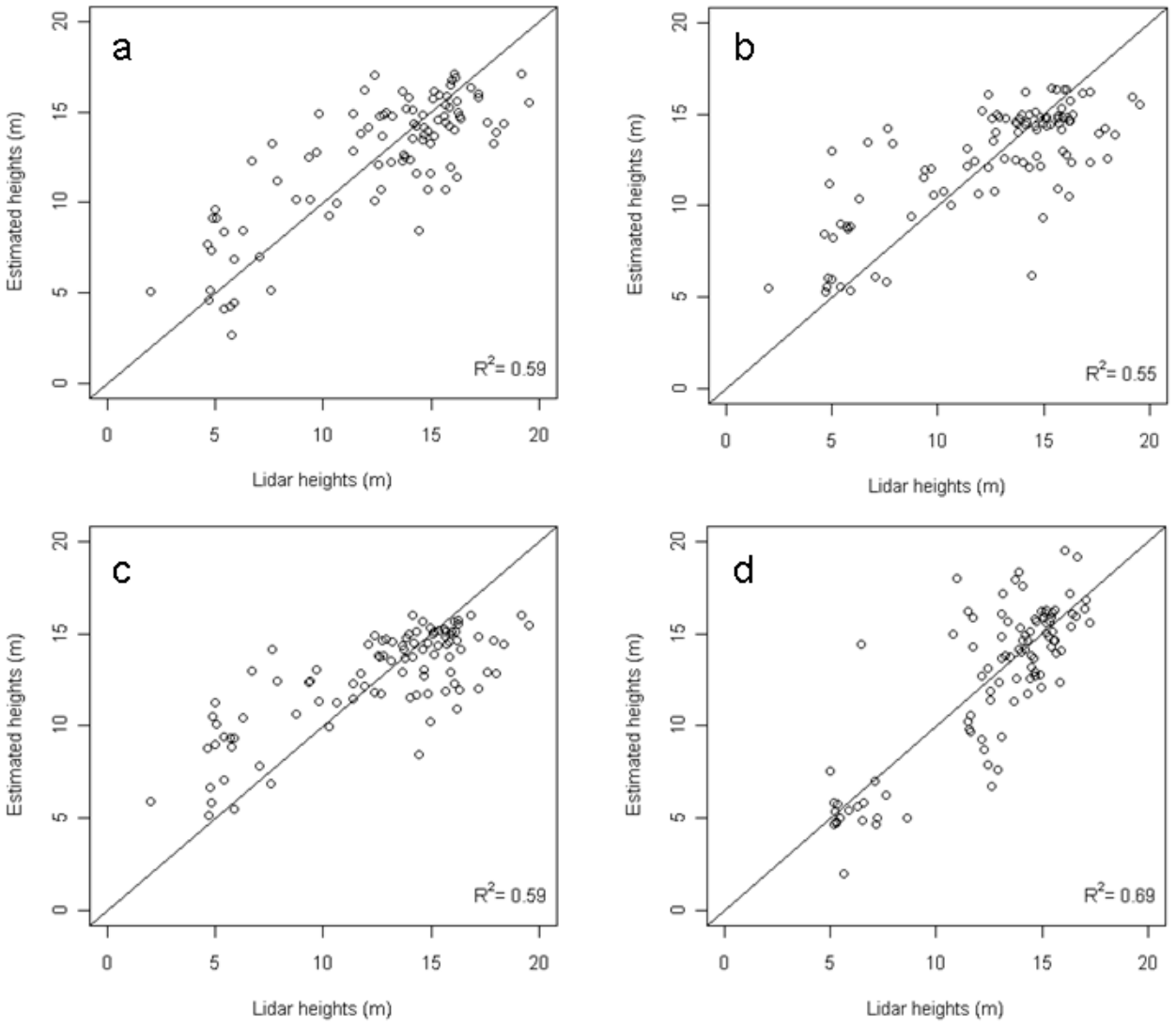

Figure 3. Residuals of the best model versus stand LIDAR height.

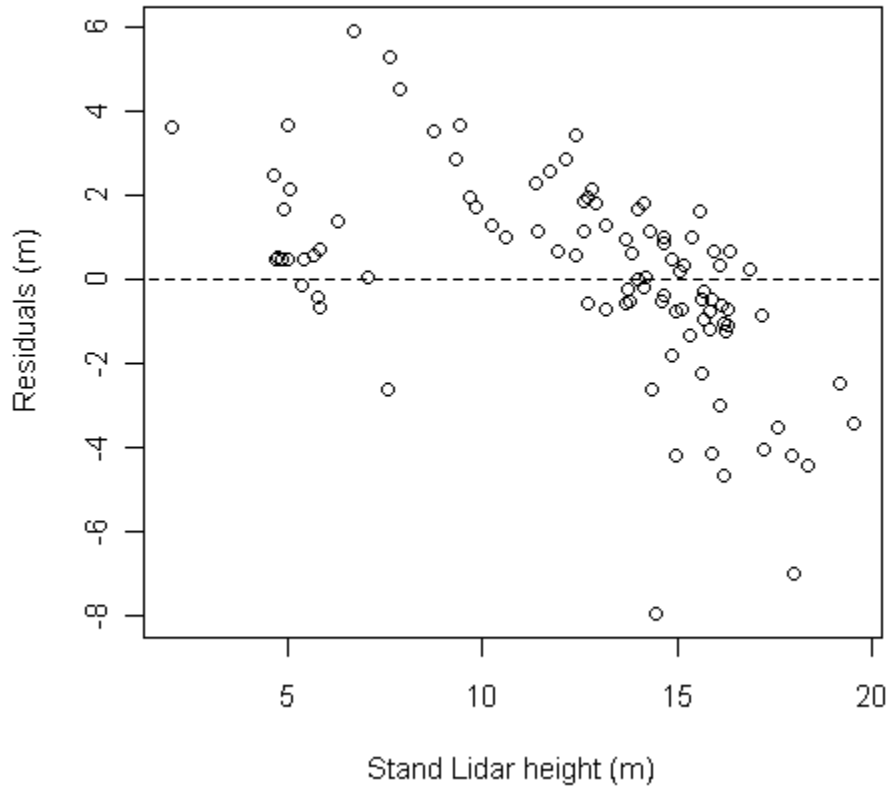

Figure 4. Residuals of the best model versus stand LIDAR height standard deviation.

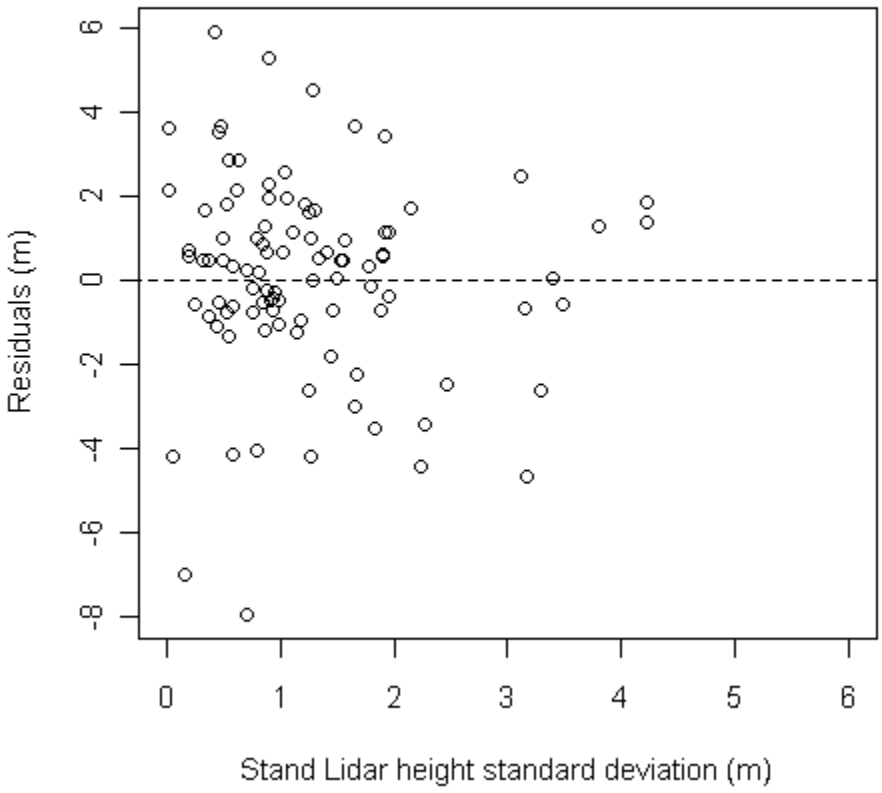

Figure 5. Variations of the standard deviation of the stand height estimates across the iterations for each model (minimum, average, and maximum)